Solid State Phenomena
ISSN: 1662-9779, Vol. 387, pp 33-41
doi:10.4028/p-fNrp4N

Submitted: 2025-12-19
Revised: 2026-02-16
Accepted: 2026-02-16
Online: 2026-04-14

Influence of Fiber Orientation Clustering Methods in Virtual Process Chains of Discontinuous-Fiber Composite Components

Louis Schreyer [a*], Luca Salvatore Pusineri Yaluff [b], Constantin Krauß [c], and Luise Kärger [d]

Karlsruhe Institute of Technology (KIT), Institute for Vehicle System Technology (FAST) – Lightweight Engineering, Rintheimer Querallee 2, 76131 Karlsruhe, Germany

[a]louis.schreyer@kit.edu, [b]luca.yaluff@student.kit.edu, [c]constantin.krauss@partner.kit.edu, [d]luise.kaerger@kit.edu

Keywords: Fiber Orientation, Clustering, Molding Simulation, Structural Simulation

Abstract. In virtual process chains for discontinuous fiber-reinforced polymers, clustering of fiber ori-entation tensors reduces the number of macroscopic material cards required for downstream structural and warpage simulations. However, it remains unclear whether including the additional information provided by the fourth-order fiber orientation tensor improves clustering quality. This study investi-gates the influence of second-order vs. fourth-order informed clustering on clustering outcomes and the resulting orientation-averaged mechanical properties. Using parameterizations based on harmonic decomposition, rotation-invariant clustering is performed in both the second-order and fourth-order parameter spaces. Results from injection molding simulation data indicate that the level of tensorial information has limited effect when the fourth-order tensor is computed via a closure approximation, as the deviatoric parameters are nonlinearly dependent on the second-order parameters. In contrast, the choice of clustering algorithm – KMeans vs. Birch – has a more pronounced influence on cluster shapes and allocations. Furthermore, we demonstrate that clustering affects orientation-averaged stiff-ness properties, with deviations most pronounced near cluster boundaries and rarely occurring tensor shapes.

1. Introduction

In virtual process chains for discontinuous fiber-reinforced polymers (DiCoFRP), the fiber orientation is obtained from mold filling simulations [1–3]. This orientation information is transferred to down-stream warpage or structural analyses using appropriate mapping techniques [4]. The local macro-scopic properties at each material point are then determined through mean-field homogenization and orientation averaging based on the corresponding (local) fiber orientation, resulting in a unique ma-terial card per material point. However, the fiber orientation field often contains regions with similar tensorial shapes. Grouping these can drastically reduce the number of required material cards – with-out compromising model fidelity – thus simplifying pre- and post-processing. An efficient description for fiber orientation is given by the fiber orientation tensor (FOT) $\boldsymbol{A}_{\langle k \rangle}$ of kth order following the works of [5] and [6]:

$$\boldsymbol{A}_{\langle k \rangle} = \int_{\mathcal{S}^2} \Psi(\boldsymbol{p}) \boldsymbol{p}^{\otimes k} \mathrm{d}S, \tag{1}$$

where $\Psi(\boldsymbol{p})$ is the fiber orientation distribution function (FODF), $\boldsymbol{p} \in \mathcal{S}^2$ describes a fiber's orientation and $\mathcal{S}^2$ is the unit sphere. Thus, the FOT represents the statistical moments of the FODF. While molding simulations generally employ the second-order FOT $\boldsymbol{A}$ for computational efficiency, orientation average of mechanical properties require fourth-order FOT $\mathbb{A}$. The latter are obtained from second-order tensors using a closure approximation.

A common approach for grouping FOT is KMeans clustering of the eigenvalues of the second-order FOT [7]. In the context of composites, the KMeans algorithm has also been applied to plastic strain data [8]. An alternative non-adaptive approach is provided by triangularization of the eigenspace [9]. However, these works do not address whether including information from the fourth-order FOT

in the clustering procedure improves the grouping quality. Similar to the influence of the closure and mapping sequence in CAE chains [10], the level of tensorial information considered may affect clustering behavior and, consequently, the accuracy of the predicted (orientation-averaged) mechanical properties. This motivates the central question of this study: Does fourth-order informed clustering, which incorporates the additional information provided by the fourth-order FOT, yield improved results compared to second-order informed clustering? To this end, we study and quantify the differences between these clustering approaches based on the resulting fourth-order FOT. Furthermore, we demonstrate the implications of clustering on the orientation-averaged linear elastic stiffnesses.

This contribution is structured as follows. First, we introduce parameterizations of the second- and fourth-order FOT based on harmonic decomposition, which enable rotation-invariant clustering. Then, we describe the clustering procedure and compare the two approaches – second-order informed and fourth-order informed clustering – using orientation fields from injection molding simulations. Finally, we discuss the implications of clustering on orientation-averaged mechanical properties.

2. Parameterization of Fiber Orientation Tensors

A parameterization of the rotation-invariant shape of the second-order FOT $\boldsymbol{A}$ is given by its eigenvalues λ_i, $i = 1..3$, with $\lambda_1 \geq \lambda_2 \geq \lambda_3$ and corresponding eigenvectors $\boldsymbol{v}_i$:

$$\boldsymbol{A}\left(\lambda_1, \lambda_2\right) = \lambda_1 \boldsymbol{v}_1 \otimes \boldsymbol{v}_1 + \lambda_2 \boldsymbol{v}_2 \otimes \boldsymbol{v}_2 + (1 - \lambda_1 - \lambda_2)\boldsymbol{v}_3 \otimes \boldsymbol{v}_3, \tag{2}$$

where we use the normalization condition $\sum_i^3 \lambda_i = 1$. Thus, the shape of $\boldsymbol{A}$ is fully described by its two largest eigenvalues λ_1 and λ_2. The admissible set of eigenvalues is known as the orientation triangle, with the extrema: unidirectional (UD; $\lambda_1 = 1$), planar isotropic ($\lambda_1 = \lambda_2 = 1/2$), and isotropic ($\lambda_i = 1/3$). The transformation between the orientation coordinate system (OCS) $\{\boldsymbol{v}_i\}$ spanned by the eigenvectors $\boldsymbol{v}_i$ of $\boldsymbol{A}$ and a fixed global coordinate system $\{\boldsymbol{e}_i\}$ is given by the orthogonal basis transformation $\boldsymbol{Q} = \boldsymbol{v}_i \otimes \boldsymbol{e}_i$.

An alternative representation of the rotation-invariant shape is given by the non-orthogonal decomposition following [11] as

$$\boldsymbol{A}\left(\alpha_1, \alpha_3\right) = \boldsymbol{A}^{\text{iso}} + \alpha_1 \boldsymbol{H}^{\text{tv}_1} + \alpha_3 \boldsymbol{H}^{\text{tv}_3}, \tag{3}$$

with $\boldsymbol{A}^{\text{iso}} = \boldsymbol{I}/3$, the second-order identity tensor $\boldsymbol{I}$, the transversely isotropic deviatoric structure tensors

$$\boldsymbol{H}^{\text{tv}_1} = \begin{pmatrix} 1 & 0 & 0 \\ & -1/2 & 0 \\ \text{sym} & & -1/2 \end{pmatrix} \boldsymbol{v}_i \otimes \boldsymbol{v}_j \quad \text{and} \quad \boldsymbol{H}^{\text{tv}_3} = \begin{pmatrix} -1/2 & 0 & 0 \\ & -1/2 & 0 \\ \text{sym} & & 1 \end{pmatrix} \boldsymbol{v}_i \otimes \boldsymbol{v}_j, \tag{4}$$

and

$$0 \leq \alpha_1 \leq 1 \quad \text{and} \quad \frac{\alpha_1}{2} - \frac{1}{3} \leq \alpha_3 \leq 0. \tag{5}$$

The isotropic state corresponds to $\alpha_1 = \alpha_3 = 0$. For positive α_1, a more aligned fiber orientation state in $\boldsymbol{v}_1$-direction is achieved, while α_3 describes the deviation towards the planar isotropic orientation in $\boldsymbol{v}_3$-direction. Visualizations of these parameterizations can be found in [11].

Based on harmonic decomposition [12, 13], [11] present a parameterization for arbitrary fourth-order FOT. This decomposition contains a constant isotropic part $\mathbb{A}^{\text{iso}} = 1/5\,\text{sym}\,(\boldsymbol{I} \otimes \boldsymbol{I})$, a deviatoric part linear in $\boldsymbol{A}$ and a deviatoric fourth-order structure tensor $\mathbb{H}$:

$$\mathbb{A} = \mathbb{A}^{\text{iso}} + (6/7)\text{sym}\,(\boldsymbol{A}' \otimes \boldsymbol{I}) + \mathbb{H}, \tag{6}$$

with the operator $\text{sym}\,(\cdot)$ denoting full index symmetrization. The deviatoric structure tensor $\mathbb{H}$ has at most nine degrees of freedom d_i, $i = 1..9$, within the OCS, corresponding to triclinic material

symmetry. Since common fourth-order closure approximations, e.g., [14], preserve the orthotropic symmetry of $\boldsymbol{A}$, we restrict to $\mathbb{H}^{\text{ortho}} = \mathbb{H}(d_1, d_2, d_3, 0, 0, 0, 0, 0, 0)$, which within a Mandel basis $\boldsymbol{B}^{\boldsymbol{v}}_{\xi}$ with $\xi = 1..6$ spanned by the OCS is defined as [11]:

$$\mathbb{H}\left(d_1, d_2, d_3\right) \cdot \left(\boldsymbol{B}^{\boldsymbol{v}}_{\xi} \otimes \boldsymbol{B}^{\boldsymbol{v}}_{\zeta}\right) = \left(\begin{array}{ccc|ccc} \frac{3}{7}\left(2\alpha_1 - \alpha_3\right) - d_1 - d_2 & \frac{1}{14}\left(\alpha_1 - 2\alpha_3\right) + d_1 & \frac{1}{14}\left(\alpha_1 + \alpha_3\right) + d_2 & 0 & 0 & 0 \\ & -\frac{3}{7}\left(\alpha_1 + \alpha_3\right) - d_1 - d_3 & \frac{1}{14}\left(-2\alpha_1 + \alpha_3\right) + d_3 & 0 & 0 & 0 \\ & & \frac{3}{7}\left(-\alpha_1 + 2\alpha_3\right) - d_2 - d_3 & 0 & 0 & 0 \\ \hline \multicolumn{3}{c|}{\text{completely}} & \multicolumn{3}{c}{\text{symmetric}} \end{array}\right). \tag{7}$$

Thus, the orientation-invariant shape of an orthotropic fourth-order FOT within the OCS is described by the five parameters: α_1, α_3, d_1, d_2, and d_3. In an engineering context, the first two parameters directly follow from the second-order FOT known from molding simulations, while the last three are estimated by an (orthotropic) closure approximation:

$$(d_1, d_2, d_3) \approx \boldsymbol{f}^{\text{Closure}}(\alpha_1, \alpha_3), \quad \boldsymbol{f} : \mathbb{R}^2 \to \mathbb{R}^3. \tag{8}$$

The nonlinear mapping of the (orthotropic) IBOF closure [14] is shown in Figure 1.

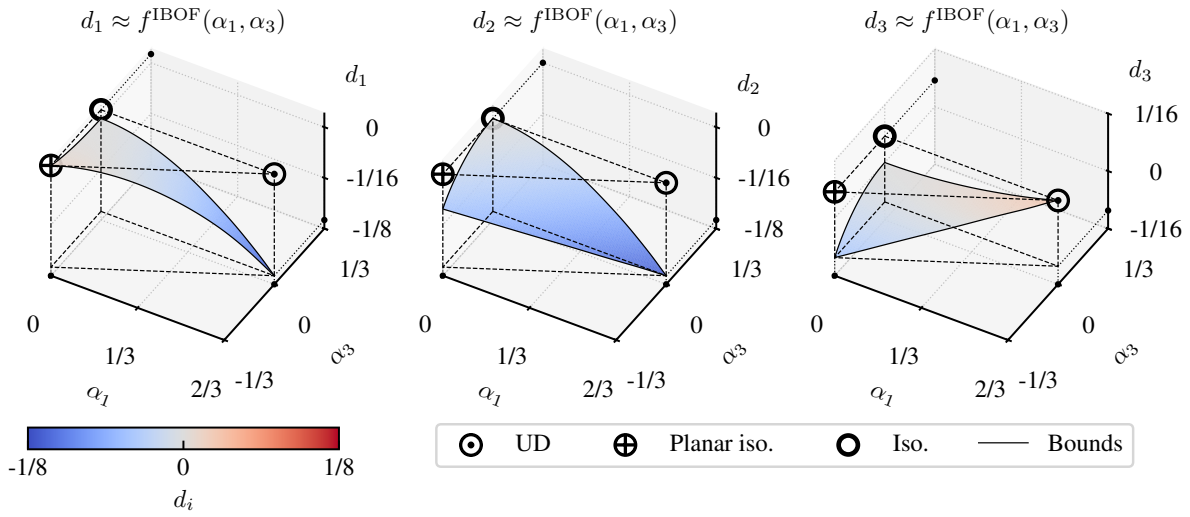

Fig. 1: Nonlinear mapping of the deviatoric parameters d_1, d_2, d_3 as a function of α_1 and α_3 for the IBOF closure [14].

3. Clustering Procedure

As discussed above, grouping FOT with similar tensorial shapes reduces the number of material cards required in downstream simulations. The two approaches for performing this data reduction are depicted in Figure 2. In both cases, the FOT field obtained from molding simulations $\boldsymbol{A}^{(\text{Src})}_I$, transformed to the OCS, is the starting point for obtaining the clustered fourth-order FOT $\hat{\mathbb{A}}^{(\text{Cluster})}_J$. In fourth-order informed clustering (top row), the fourth-order fiber orientation tensor $\mathbb{A}^{(\text{Src})}_I$ is first approximated via a closure, which then serves as input for clustering. In contrast, in second-order informed clustering (bottom row), $\boldsymbol{A}^{(\text{Src})}_I$ is clustered directly, and the closure is subsequently applied to the clustered second-order FOT $\hat{\boldsymbol{A}}^{(\text{Cluster})}_J$ to obtain $\hat{\mathbb{A}}^{(\text{Cluster})}_J$. Depending on the order of the FOT, either $(\alpha_1, \alpha_3, d_1, d_2, d_3)$

(top row) or (α_1, α_3) (bottom row) are clustered. Alternatively, the eigenvalue-based parameterization (λ_1, λ_2) can be used instead of (α_1, α_3); however, as the conversion between the eigenspace- and harmonic-parameterizations is (linear) oblique, mixing notations between second- and fourth-order clustering does not permit a fair comparison.

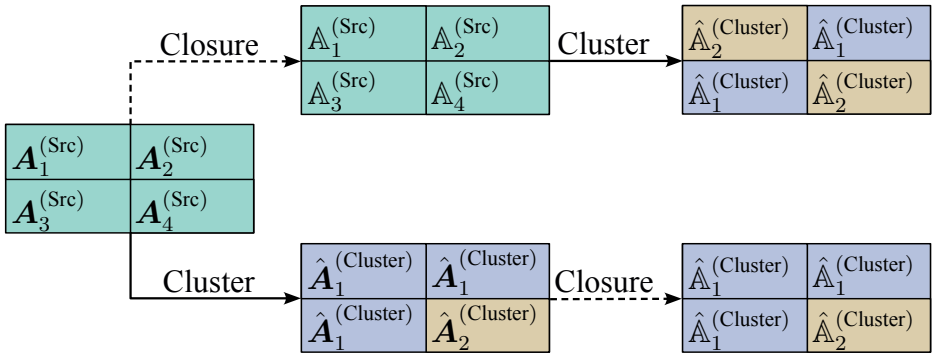

Fig. 2: Possible clustering routes in virtual process chains. Fourth-order informed clustering is depicted in the top row and the bottom row shows second-order informed clustering.

In the following section, we present clustering results for the two approaches depicted in Figure 2 utilizing second-order FOT data from an injection molding simulation dataset [15], which comprises 629 part geometries ranging from plate-like shapes to complex three-dimensional structures, such as a mounting bracket. The fourth-order FOT is approximated using the IBOF closure [14]. In addition to the influence of the level of tensorial information, we also discuss the influence of the clustering algorithm. In this work, the KMeans [16, 17] and Birch [18] clustering algorithms available within the *scikit-learn* Python package [19] are considered. The KMeans algorithm minimizes the within-cluster sum-of-squares, i.e., the sum of squared Euclidean distances between each data point and its corresponding cluster centroid. The Birch algorithm builds a hierarchical tree structure by incrementally inserting data points into subclusters, which are then aggregated to form the final clusters. This approach is memory-efficient and scales well to large orientation fields.

4. Results and Discussion

Influence of level of tensorial information. We investigate the influence of the level of tensorial information (second-order vs. fourth-order informed clustering) based on clustering results for several parts with $n = 10$ clusters, as depicted in Figure 3. The results are visualized in the eigenspace, as this representation is more widely used. The colors indicate cluster affiliation, and the ”X” markers denote the corresponding cluster centroids. For consistent coloring across different clustering methods, colors are assigned based on the centroid’s λ_1 value. The probability density functions (PDF) of each cluster in λ_1 and λ_2 are shown on the top and right axes, respectively. The selected parts exhibit distinctive geometrical features, resulting in different distributions of (rotation-invariant) fiber orientation shapes. For the parts in the upper two rows, the second- and fourth-order clustering results (first two columns) yield similar cluster centroids and allocations. Only the results for the bottom row part show notable differences, which can be attributed to two reasons. First, the deviatoric parameters d_1, d_2, d_3 span a smaller range than α_1 and α_3 (cf. Figure 1), causing the latter to dominate the within-cluster variance. This bias could be mitigated through parameter normalization; however, normalization is not considered in this study. Second, the deviatoric parameters d_1, d_2, d_3 depend nonlinearly on α_1 and α_3, and are thus not independent. As a result, the dimensionality does not increase when including the deviatoric parameters; instead, the two-dimensional space spanned by α_1 and α_3 becomes curved (cf. Equation 8). A true increase in dimensionality would require omitting the closure approximation, thereby allowing general orthotropic states – for instance, by reconstructing the fourth-order FOT directly from the FODF. The extreme case is represented by triclinic orientation states.

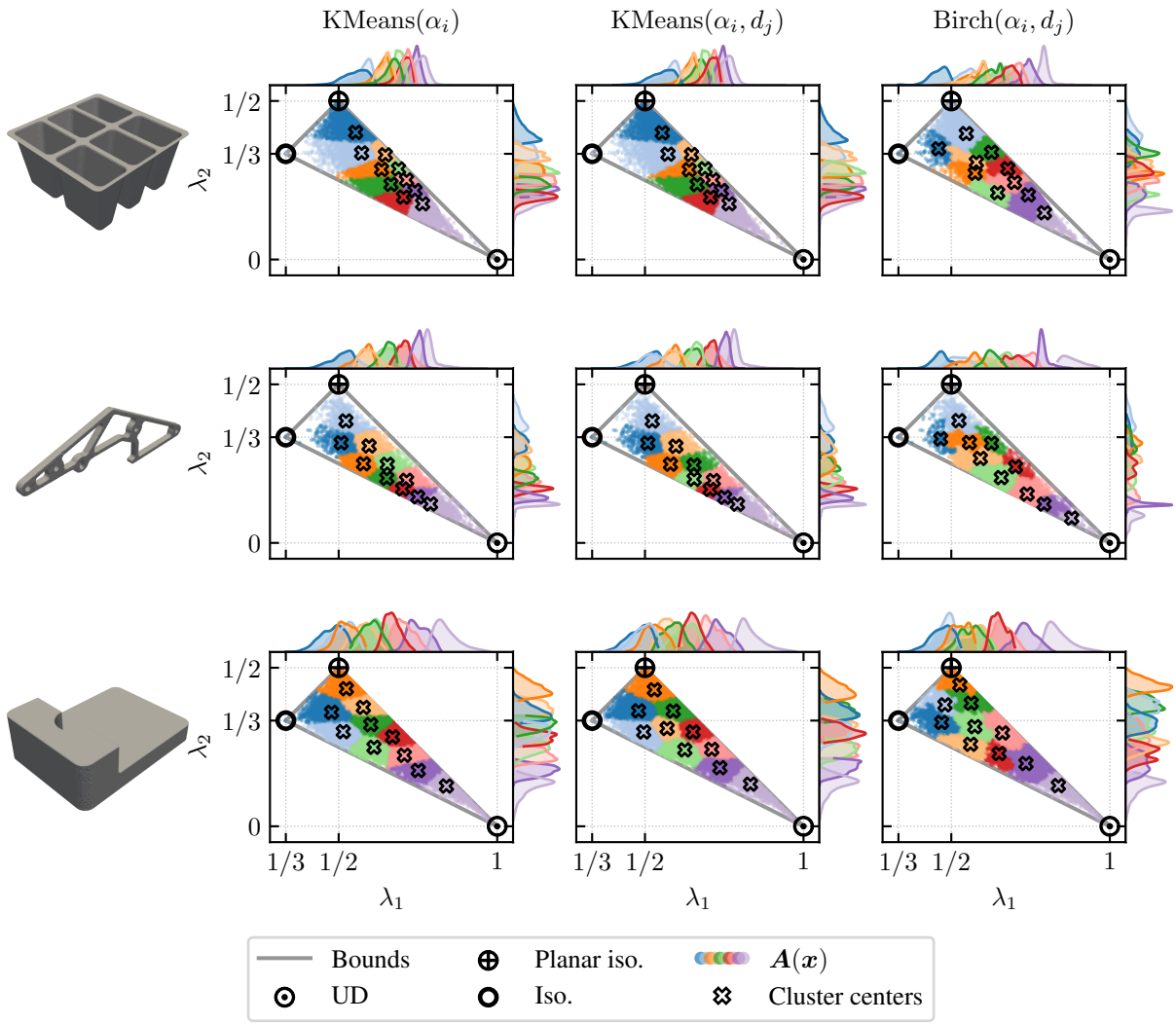

Fig. 3: Results of KMeans and Birch clustering for α_1, α_3 (second-order informed; first column) and $\alpha_1, \alpha_3, d_1, d_2, d_3$ (fourth-order informed; second and third column) with $n = 10$ clusters for three injection-molded part geometries (top, center, bottom) from the molding dataset [15]. The coloring represents cluster allocation and is sorted by the cluster centroid's λ_1 value. The corresponding probability density functions in λ_1 and λ_2 are shown on the top and right axes.

Influence of clustering algorithm. Compared to the differences between the levels of tensorial information (due to the implications of the closure), the choice of clustering algorithm has a more pronounced effect on the outcome (cf. second vs. third column in Figure 3). This stems from fundamental algorithmic differences. KMeans iteratively minimizes the within-cluster variance, whereas Birch incrementally builds a hierarchical tree structure based on a threshold parameter. As a result, the Birch algorithm may produce clusters with more irregular shapes and higher variance, as evident in the PDF of the first two rows of Figure 3.

Influence of number of clusters. An important free parameter is the number of clusters n. In Figure 3, a small number of clusters is chosen deliberately to emphasize the differences between methods. To quantify the deviation between individual data points and their associated cluster centroids, we introduce the following relative measure:

$$\|\Delta\mathbb{A}\| = \frac{\|\mathbb{A} - \mathbb{A}^{\text{Cluster}}\|}{\|\mathbb{A}\|}. \tag{9}$$

Clearly, as $n \to n_\mathrm{s}$, $\|\Delta\mathbb{A}\| \to 0$, where n_s denotes the total number of data points of the simulation. The required number of clusters depends on the component geometry and the fiber-flow interaction. Accordingly, fewer clusters are needed to adequately represent the (rotation-invariant) FOT field in a geometrically simple part (e.g., a plate) compared to a complex one. Figure 4 shows clustering results using fourth-order informed clustering with KMeans for the part in the second row of Figure 3, with $n \in \{50, 100, 200\}$ clusters. Elements exceeding thresholds of 5 %, 10 %, and 15 % are marked in red. As expected, the number of flagged elements decreases with increasing threshold and with a larger number of clusters. Notably, the flagged elements are predominantly located at complex geometrical features. This can be explained by two factors. First, the mesh is quasi-uniform, and second, each data point is weighted equally during clustering. Consequently, regions with complex geometry have limited influence on the within-cluster variance. However, these regions are often prone to stress concentrations, e.g., due to notch effects. This issue could potentially be addressed by assigning higher weights to data points in such regions.

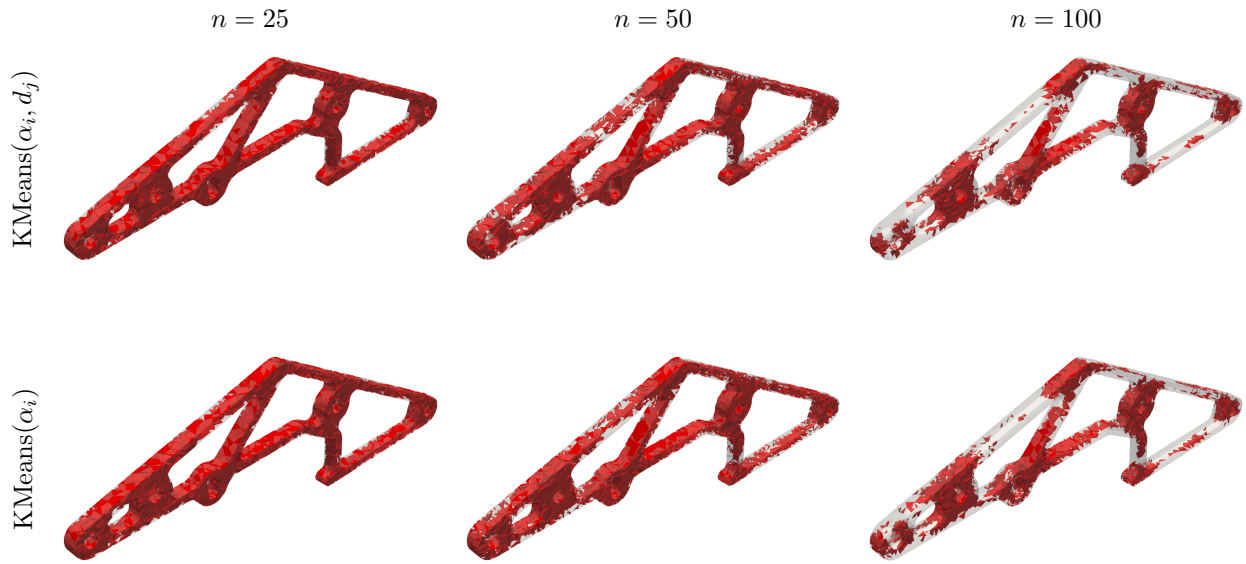

Fig. 4: Influence of number of clusters for fourth-order informed clustering using the KMeans algorithm. Red-marked regions exceed the relative deviation threshold $\|\Delta\mathbb{A}\|$ of 5 %, 10 %, or 15 %. The simulation model comprises 111,931 tetrahedral elements.

Implications on mechanical properties. Finally, we examine the influence of the clustering on the orientation-averaged mechanical properties. Figure shows the orientation-dependent Young's modulus $E(\boldsymbol{s}) = ((\boldsymbol{s} \otimes \boldsymbol{s}) \cdot \mathbb{C}^{-1}[\boldsymbol{s} \otimes \boldsymbol{s}])^{-1}$, where $\boldsymbol{s} \in \mathcal{S}^2$ is a unit direction, at sample locations P_i for a generic GF-PP DiCoFRP with an aspect ratio of 50 and a fiber mass content of 30 %. The composite's effective transversely isotropic mechanical properties are obtained via mean-field homogenization following [20], and the orientation average is computed according to [6]. The sample points are selected to highlight differences arising from the clustering approach (second-order vs. fourth-order informed) and the choice of clustering algorithm. Note that increasing the fiber aspect ratio amplifies the anisotropy of the orientation-averaged Young's modulus.

Pronounced variations in the Young's modulus occur at data points located near cluster boundaries. This effect is particularly evident for data points with highly aligned fiber orientations ($\lambda_1 \to 1$; gray-colored cluster in Figure). Depending on the level of tensorial information or the clustering algorithm, a data point's assigned centroid may correspond to a more isotropic or more aligned state. For instance, at sample point P_3, the Young's modulus exhibits stronger anisotropy for second-order informed clustering (first column) compared to fourth-order informed clustering (second column).

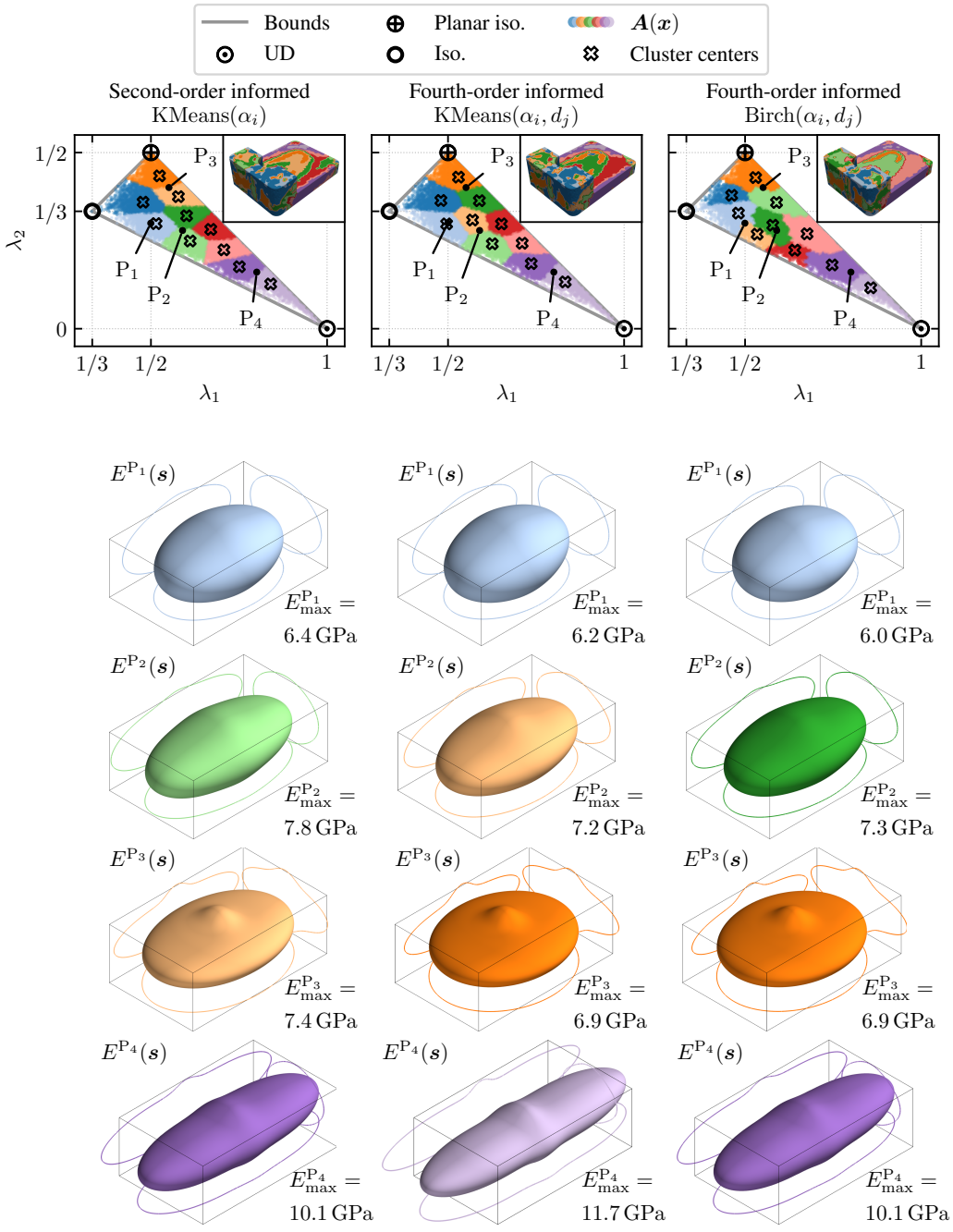

Fig. 5: Influence of tensorial information level (first two columns) and clustering algorithm (last two columns) on the orientation-averaged fourth-order stiffness tensor $\langle \mathbb{C}(\mathbb{A}) \rangle_{S^2}$ at sample positions P_i of the part depicted in the bottom row of Figure 3. The first row shows the clustering results in the eigenspace and the corresponding part colored by cluster labels. Subsequent rows display the stiffness bodies $E^{P_i}(\boldsymbol{s})$ [21] of the cluster centroids in the OCS $\{\boldsymbol{v}_i\}$. Colors represent cluster allocation and are sorted by the centroid's λ_1 value.

The clustering of FOT thus affects the predicted stress distribution in structural simulations and the formation of residual stresses in warpage simulations. These results further indicate that global scalar metrics, such as mean squared error or Euclidean distance, are insufficient for evaluating clustering quality, as they disregard directional and spatial information.

5. Conclusion

This study investigates the influence of the level of tensorial information – second-order vs. fourth-order informed – on fiber orientation tensor clustering in virtual process chains for discontinuous fiber-reinforced polymers. Using parameterizations based on harmonic decomposition, we enable rotation-invariant clustering in both the second-order (α_1, α_3) and fourth-order (α_1, α_3, d_1, d_2, d_3) parameter spaces.

The results indicate that the level of tensorial information has a limited effect on clustering outcomes when the fourth-order fiber orientation tensor is derived from the second-order tensor via an (orthotropic) closure approximation. This is attributed to the nonlinear dependence of the deviatoric parameters d_1, d_2, d_3 on the second-order fiber orientation tensor parameters α_1 and α_3 imposed by the closure approximation, which effectively curves the parameter space rather than increasing its dimensionality. In addition, the deviatoric parameters span a small range relative to α_1 and α_3. In contrast, the choice of clustering algorithm – KMeans vs. Birch – has a more pronounced influence on cluster shapes and allocations.

The question of which clustering approach yields superior results cannot be answered definitively. However, from a theoretical standpoint, fourth-order informed clustering should be preferred, as it incorporates additional information from the closure approximation. The alternative – clustering in the second-order space and subsequently applying the closure – effectively discards this information and relies on estimating the deviatoric parameters from the cluster centroids.

Furthermore, we demonstrated that clustering affects orientation-averaged mechanical properties, with pronounced deviations occurring near cluster boundaries and low-occurrence tensor shapes. Global metrics such as mean squared error or Euclidean distance are insufficient for evaluating clustering quality, as they do not account for directionality or spatial position. Future work could address this limitation by incorporating directional error measures or by introducing spatially weighted clustering schemes that prioritize regions prone to stress concentrations.

Acknowledgements

The research documented in this manuscript has been funded initially by the German Federal Ministry for Economic Affairs and Climate Action (BMWK) as part of the EcoDynamicSMC research project, and subsequently by the German Research Foundation (DFG) as part of the project MeproSi (project no.: 464119659). The work is also part of the Heisenberg project ”Digitalization of fiber-reinforced polymer processes for resource-efficient manufacturing of lightweight components” (455807141), funded by the DFG. The support by the DFG and BMWK is gratefully acknowledged.

References

[1] F. Wittemann, R. Maertens, L. Kärger, and F. Henning, “Injection molding simulation of short fiber reinforced thermosets with anisotropic and non-Newtonian flow behavior,” *Composites Part A: Applied Science and Manufacturing*, vol. 124, p. 105476, Sept. 2019.

[2] J. Görthofer, N. Meyer, T. D. Pallicity, L. Schöttl, A. Trauth, M. Schemmann, M. Hohberg, P. Pinter, P. Elsner, F. Henning, A. N. Hrymak, T. Seelig, K. Weidenmann, L. Kärger, and T. Böhlke, “Virtual process chain of sheet molding compound: Development, validation and perspectives,” *Composites Part B: Engineering*, vol. 169, pp. 133–147, July 2019.

[3] P. Kennedy and R. Zheng, *Flow analysis of injection molds*. Carl Hanser Verlag GmbH & Co. KG, Apr. 2013.

[4] C. Krauß and L. Kärger, “Tensor interpolation in virtual manufacturing chains for fiber reinforced composites,” *International Journal of Mechanical Sciences*, vol. 226, p. 107378, July 2022.

[5] K.-I. Kanatani, "Distribution of directional data and fabric tensors," *International Journal of Engineering Science*, vol. 22, pp. 149–164, Jan. 1984.
[6] S. G. Advani and C. L. Tucker, "The use of tensors to describe and predict fiber orientation in short fiber composites," *Journal of Rheology*, vol. 31, pp. 751–784, Nov. 1987.
[7] M. Hohberg, *Experimental investigation and process simulation of the compression molding process of sheet molding compound (SMC) with local reinforcements*. PhD thesis, Karlsruhe Institute of Technology (KIT), Germany, 2022.
[8] V. Romanenko, *Materialcharakterisierung und durchgängige 3D-Prozesssimulation für kohlenstofffaserverstärktes Sheet Molding Compound*. PhD thesis, RPTU University Kaiserslautern-Landau, Kaiserslautern, 2021.
[9] J. Köbler, M. Schneider, F. Ospald, H. Andrä, and R. Müller, "Fiber orientation interpolation for the multiscale analysis of short fiber reinforced composite parts," *Computational Mechanics*, vol. 61, no. 6, pp. 729–750, 2018.
[10] C. Krauß, J. K. Bauer, J. Mitsch, T. Böhlke, and L. Kärger, "On the averaging and closure of fiber orientation tensors in virtual process chains," *Journal of Elasticity*, vol. 156, pp. 279–306, Aug. 2024.
[11] J. K. Bauer and T. Böhlke, "Variety of fiber orientation tensors," *Mathematics and Mechanics of Solids*, vol. 27, no. 7, pp. 1185–1211, 2022.
[12] S. Forte and M. Vianello, "Symmetry classes for elasticity tensors," *Journal of Elasticity*, vol. 43, pp. 81–108, May 1996.
[13] J. Rychlewski, "A qualitative approach to Hooke's tensors. Part I," *Archives of Mechanics*, vol. 52, pp. 737–759, Jan. 2000.
[14] D. H. Chung and T. H. Kwon, "Invariant-based optimal fitting closure approximation for the numerical prediction of flow-induced fiber orientation," *Journal of Rheology*, vol. 46, no. 1, pp. 169–194, 2002.
[15] N. Meyer and J. Greif, "Injection molding simulations," May 2024.
[16] J. MacQueen, "Multivariate observations," in *Proceedings of the 5th Berkeley symposium on mathematical statistics and probability*, vol. 1, pp. 281–297, 1967.
[17] S. Lloyd, "Least squares quantization in PCM," *IEEE transactions on information theory*, vol. 28, no. 2, pp. 129–137, 1982.
[18] T. Zhang, R. Ramakrishnan, and M. Livny, "BIRCH: An efficient data clustering method for very large databases," *SIGMOD Rec.*, vol. 25, pp. 103–114, June 1996.
[19] F. Pedregosa, G. Varoquaux, A. Gramfort, V. Michel, B. Thirion, O. Grisel, M. Blondel, P. Prettenhofer, R. Weiss, V. Dubourg, J. Vanderplas, A. Passos, D. Cournapeau, M. Brucher, M. Perrot, and É. Duchesnay, "Scikit-learn: Machine learning in Python," *Journal of Machine Learning Research*, vol. 12, no. 85, pp. 2825–2830, 2011.
[20] G. P. Tandon and G. J. Weng, "The effect of aspect ratio of inclusions on the elastic properties of unidirectionally aligned composites," *Polymer Composites*, vol. 5, pp. 327–333, Oct. 1984.
[21] T. Böhlke and C. Brüggemann, "Graphical representation of the generalized Hooke's law," *Technische Mechanik*, vol. 21, no. 2, p. 145, 2001.

The publication of this article was funded by the Karlsruhe Institute of Technology 10.13039/100009133